Turkish Journal of Engineering & Environmental Sciences

http://journals.tubitak.gov.tr/engineering/

Research Article

Turkish J Eng Env Sci
(2014) 38: 309 - 322

doi:10.3906/muh-1211-5

Successive approximation method for time-dependent creep modeling of functionally graded piezoelectric cylinder

Ali GHORBANPOUR ARANI[1,2,*], **Reza KOLAHCHI**[1]

[1]Faculty of Mechanical Engineering, University of Kashan, Kashan, Iran

[2]Thermoelasticity Center of Excellence, Department of Mechanical Engineering, Amirkabir University of Technology, Tehran, Iran

Received: 06.11.2012 • **Accepted/Published Online:** 26.10.2014 • **Printed:** 04.03.2016

Abstract: Time-dependent creep behavior of hollow rotating cylinders made from functionally graded piezoelectric material has been investigated using Mendelson's method of successive approximation. All the mechanical, thermal, and piezoelectric properties are modeled as the power-law distribution of volume fraction. Based on equilibrium, strain displacement, stress-strain, and electric displacement relations, a differential equation containing creep strains for displacement is derived. Creep strains are time-, temperature-, and stress-dependent, and the closed-form solution cannot be found for this constitutive differential equation. A semianalytical method in conjunction with the method of successive approximation has therefore been proposed for this analysis. Similar to the radial stress histories, electric potentials increase with time, because the latter is induced by the former during creep deformation of the cylinder, justifying industrial application of such a material as efficient actuators and sensors.

Key words: Successive approximation method, time-dependent creep, cylinder, functionally graded, piezoelectric

1. Introduction

Piezoelectric effect has important uses in modern engineering because it expresses the connection between the electrical and mechanical fields, which has wide applications in electromechanical devices such as actuators, sensors, and transducers. Recently, a new class of composite materials known as functionally graded materials (FGMs) has drawn considerable attention. A typical FGM, with a high bending–stretching coupling effect, is an inhomogeneous composite made from different phases of material constituents (usually ceramic and metal).

The first idea for producing FGMs was their application in high-temperature environments and improving their mechanical properties. These materials, which are mainly constructed to operate in high-temperature environments, find applications in nuclear reactors, chemical laboratories, aerospace engineering, turbine rotors, flywheels, and pressure vessels. As the use of FGMs increases, new methodologies need to be developed to characterize, analyze, and design structural components made of these materials.

Thermoelectroelastic analysis of functionally graded piezoelectric material (FGPM) components has been investigated by many researchers. Mechanical and thermal stresses in a functionally graded hollow cylinder were investigated by Jabbari et al. [1]. Analysis of the thermal stress behavior of functionally graded hollow circular cylinders was presented by Liew et al. [2]. You et al. [3] presented elastic analysis of internally pressurized thick-walled spherical pressure vessels of functionally graded materials. Dai et al. [4] studied exact solutions

*Correspondence: aghorban@kashanu.ac.ir

for functionally graded pressure vessels in a uniform magnetic field. Coupled thermoelasticity of functionally graded cylindrical shells was developed by Bahtui and Eslami [5]. Recently, Ghorbanpour Arani et al. [6] investigated the effect of material inhomogeneity on electrothermomechanical behaviors of a functionally graded piezoelectric rotating shaft. They also studied electrothermomechanical behaviors of FGPM spheres using an analytical method and ANSYS software [7].

None of the above studies considered creep deformation of FGPM cylinders. Pai [8] investigated steady-state creep analysis of thick-walled orthotropic cylinders. Sim and Penny [9] analyzed plane strain creep behavior of thick-walled cylinders. Bhatnagar and Arya [10] investigated large strain creep deformation of a thick-walled cylinder of an anisotropic material subjected to internal pressure. Simonian [11] calculated the thermal stresses in thick-walled cylinders, taking account of nonlinear creep. Yang [12] presented a solution for time-dependent creep behavior of FGM cylinders using Norton's law for a material creep constitutive model. Steady-state creep of a pressurized thick cylinder in both the linear and the power law ranges was investigated by Altenbach et al. [13]. Loghman et al. [14] studied the magnetothermoelastic creep analysis of functionally graded cylinders. They found that radial stress redistributions are not significant for different material properties; however, major redistributions occur for circumferential and effective stresses. Later, Loghman et al. [15] studied magnetothermoelastic creep behavior of thick-walled FGM spheres placed in uniform magnetic and distributed temperature fields and subjected to an internal pressure. They showed that stresses, strains, and effective creep strain rate are changing in time with a decreasing rate so that after almost 50 years the time-dependent solution approaches the steady-state condition. However, the cylinder and sphere materials used in [14,15] are not smart. Additionally, mechanical properties, except Poisson's ratio, through the radial graded direction are assumed to obey simple power law variation. The semianalytical solution of time-dependent electrothermomechanical creep for a radially polarized piezoelectric cylinder was investigated by Ghorbanpour Arani et al. [16] using the method of successive elastic solution. They found that, similar to the radial stress histories, electric potentials increase with time. However, they did not consider FGM for the cylinder. Recently, time-dependent behaviors of a FGPM hollow sphere under the coupling of multifields were presented by Dai et al. [17]. They assumed that material properties, electric parameters, permeability, thermal conductivity, and creep parameters varied smoothly through the radial direction of the FGPM spherical structure according to a simple power law. Recently, electrothermomechanical creep and time-dependent behaviors of FGPM spheres were investigated by Ghorbanpour Arani et al. [18].

Apart from a couple of studies, prepared by a few authors here, little or no reference has been made so far in the literature to the time-dependent creep analysis of FGPM cylinders. It was shown by Zhou and Kamlah [19] that even at room temperature ferroelectric piezoceramics exhibit significant creep effects. This creep is of a primary type and can be expressed by a power law constitutive model. To improve the performance and reliability of piezoactuators used for high-precision applications, time-dependent creep analysis must be considered when these devices are used, even at room temperatures.

To date, no report has been found in the literature on the time-dependent creep behavior of hollow rotating FGPM cylinders based on the power-law distribution of volume fraction for mechanical, thermal, and piezoelectric properties. Motivated by these considerations, we aim to investigate the history of stresses, strains, deformation, and electric potential of a thick hollow FGPM rotating cylinder made of radially polarized anisotropic piezoelectric material using a semianalytical method based on Mendelson's method of successive elastic solution.

2. Property gradation

In this study, all mechanical, thermal, and electrical properties except Poisson's ratio are assumed to be in the following form:

$$Q(r) = (Q_o - Q_i)(\frac{r-a}{b-a})^n + Q_i, a < r < b, \tag{1}$$

where Q_i, Q_o are the properties at the inner and outer surfaces of the cylinder and a and b are the inner and outer radii of the cylinder, respectively. Here the function $Q(r)$ is abbreviated as Q_r. In this study $n \geq 0$ (grading index) is the volume fraction exponent that indicates the material variation profile along the radius.

3. Basic formulation

A hollow axisymmetric FGPM cylinder rotating about its axis at constant angular velocity ω with inner and outer radius of a and b subjected to an inner pressure, thermal gradient, and electric potential is considered (Figure 1). The dimensionless constitutive relations of cylindrically orthotropic radially polarized piezoelectric media and the component of radial electric displacement vector can be written as [7, 20]:

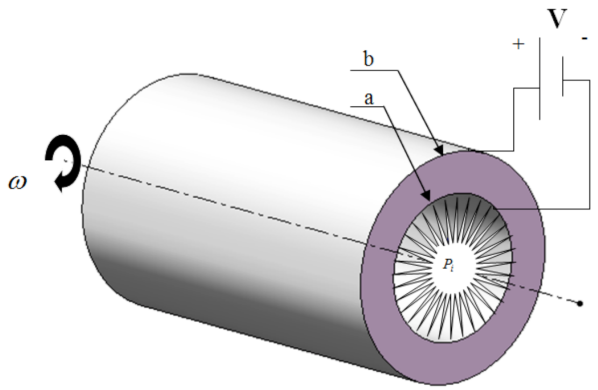

Figure 1. Hollow FGPM rotating circular shaft subject to uniform temperature field, uniform internal pressure, uniform external pressure, and applied voltage (V).

$$\sigma_r = \left(c_1\frac{\partial u}{\partial \xi} + c_2\frac{u}{\xi} - c_1\varepsilon_\xi^c - c_2\varepsilon_\theta^c - (c_1\alpha_\xi + c_2\alpha_\theta)T(\xi) + E_1\frac{\partial \Phi}{\partial \xi}\right), \tag{2}$$

$$\sigma_\theta = \left(c_2\frac{\partial u}{\partial \xi} + \frac{u}{\xi} - c_2\varepsilon_\xi^c - \varepsilon_\theta^c - (c_2\alpha_\xi + \alpha_\theta)T(\xi) + E_2\frac{\partial \Phi}{\partial \xi}\right), \tag{3}$$

$$D_r = \left(E_1\frac{\partial u}{\partial \xi} + E_2\frac{u}{\xi} - E_1\varepsilon_\xi^c - E_2\varepsilon_\theta^c - (E_1\alpha_\xi + E_2\alpha_\theta)T(\xi) - \frac{\partial \Phi}{\partial \xi}\right), \tag{4}$$

where dimensionless parameters are

$$\begin{gathered}\sigma_i = \frac{\sigma_{ii}}{c_{22}}\ (i = r, \theta), c_i = \frac{C_{1i}}{C_{22}}\ (i = 1, 2), E_i = \frac{e_{1i}}{\sqrt{C_{22}\ \in_{11}}}\ (i = 1, 2), D_r = \frac{D_{rr}}{\sqrt{C_{22}\ \in_{11}}}, \\ u = \frac{u_r}{a}, \quad \xi = \frac{r}{a}, \quad \eta = \frac{b}{a}, \quad \Omega = \frac{a^2\rho_0\omega^2}{C_{22}}, \quad \Phi = \frac{\varphi}{a\sqrt{\frac{C_{22}}{\in_{11}}}},\end{gathered} \tag{5}$$

where σ_{ii} $(i = r, \theta)$, D_{rr}, c_{ij} $(i, j = 1, 2)$, $e_{1i}(i = 1, 2), \in_{11}, \alpha_i$ $(i = r, \theta)$, and $T(\xi)$ are stress tensor, electric displacement, elastic constants, piezoelectric constants, dielectric constants, thermal expansion coefficients, and temperature gradient, respectively.

Using the above dimensionless variables, the equation of equilibrium considering the inertia body force and Maxwell's equation for free electric charge density are expressed in dimensionless form as [18]:

$$\frac{\partial \sigma_r}{\partial \xi} + \frac{\sigma_r - \sigma_\theta}{\xi} + \Omega \xi = 0, \tag{6}$$

$$\frac{\partial D_r}{\partial \xi} + \frac{D_r}{\xi} = 0. \tag{7}$$

The solution of Eq. (7) is

$$D_r = \frac{F_1}{\xi}, \tag{8}$$

where F_1 is a constant. Substituting Eq. (8) into Eq. (4), we obtain

$$\frac{\partial \Phi}{\partial \xi} = -\frac{F_1}{\xi}\xi^{-\gamma} + E_1 \frac{\partial u}{\partial \xi} + E_2 \frac{u}{\xi} - E_1 \varepsilon_\xi^c - E_2 \varepsilon_\theta^c - (E_1 \alpha_\xi + E_2 \alpha_\theta) T(\xi). \tag{9}$$

Substituting Eq. (9) into Eqs. (3) and (2) leads to

$$\sigma_r = \left(\left(C_1 + E_1^2\right) \left(\frac{\partial u}{\partial \xi} - \varepsilon_\xi^c - \alpha_\xi T(\xi) \right) + (C_2 + E_1 E_2) \left(\frac{u}{\xi} - \varepsilon_\theta^c - \alpha_\theta T(\xi) \right) - \frac{E_1 F_1}{\xi} \xi^{-\gamma} \right), \tag{10}$$

$$\sigma_\theta = \left((C_2 + E_1 E_2) \left(\frac{\partial u}{\partial \xi} - \varepsilon_\xi^c - \alpha_\xi T(\xi) \right) + \left(1 + E_2^2\right) \left(\frac{u}{\xi} - \varepsilon_\theta^c - \alpha_\theta T(\xi) \right) - \frac{E_2 F_1}{\xi} \xi^{-\gamma} \right). \tag{11}$$

Electric potential Φ is obtained by integrating Eq. (9):

$$\Phi = \int \left(E_1 \frac{\partial u}{\partial \xi} + E_2 \frac{u}{\xi} - E_1 \varepsilon_\xi^c - E_2 \varepsilon_\theta^c - (E_1 \alpha_\xi + E_2 \alpha_\theta) T(\xi) - \frac{F_1}{\xi} \xi^{-\gamma} \right) d\xi. \tag{12}$$

To obtain the equilibrium equation in terms of the displacement for the functionally graded rotating cylinder, the functional relationships of the material properties have to be known. The variation of property along the radius, as explained in Section 2, is a power-law distribution of volume fraction as follows:

$$\begin{aligned}
c_\xi &= c(\xi) = (c_o - c_i)\left(\frac{\xi - 1}{\eta - 1}\right)^m + c_i, \\
\alpha_\xi &= \alpha(\xi) = (\alpha_o - \alpha_i)\left(\frac{\xi - 1}{\eta - 1}\right)^m + \alpha_i, \\
\rho_\xi &= \rho(\xi) = (\rho_o - \rho_i)\left(\frac{\xi - 1}{\eta - 1}\right)^m + \rho_i, \\
E_\xi &= E(\xi) = (E_o - E_i)\left(\frac{\xi - 1}{\eta - 1}\right)^m + E_i.
\end{aligned} \tag{13}$$

Finally, substituting Eqs. (10) and (11) into Eq. (6) yields a nonhomogeneous second-order ordinary differential equation containing time-dependent creep strains for displacement field in the FGPM hollow rotating cylinder, which is discussed in next section.

4. Semianalytical solution

A semianalytical method for solution of the differential equation has been applied. The solution domain is first divided into some finite divisions, as shown in Figure 2. The coefficients of the differential equation are evaluated at ξ^m, the mean radius of mth division, and therefore the differential equation with constant coefficients becomes valid only for the mth subdomain, which can be rewritten as [21, 22]:

$$\left(P_1^m \frac{d^2}{dr^2} + P_2^m \frac{d}{dr} + P_3^m\right) u^m + P_4^m = 0, \tag{14}$$

$$P_1^m = (\xi^m)^2, \tag{15}$$

$$P_2^m = \left(\left.\frac{d\, c_1(\xi^m)}{d\xi^m}\right|_{\xi=\xi^m} + \frac{c_1(\xi^m) + E_1(\xi^m)^2}{\xi^m} + 2E_1(\xi^m) \left.\frac{d\, E_1(\xi^m)}{d\xi^m}\right|_{\xi=\xi^m} \right) / \left(c_1(\xi^m) + E_1(\xi^m)^2\right) \Bigg) \xi^m, \tag{16}$$

$$P_3^m = \left(\xi^m \left(\left.\frac{d\, c_1(\xi^m)}{d\xi^m}\right|_{\xi=\xi^m} + \left.\frac{d}{d\xi^m}\left(E_1(\xi^m)E_2(\xi^m)\right)\right|_{\xi=\xi^m} \right) - \left(1 + E_2(\xi^m)^2\right) \right) / \left(c_1(\xi^m) + E_1(\xi^m)^2\right), \tag{17}$$

$$\begin{aligned} P_4^m \;=\; & (\xi^m)^2 \left(\left(\left.\tfrac{d\, c_1(\xi^m)}{d\xi^m}\right|_{\xi=\xi^m} + 2E_1(\xi^m) \left.\tfrac{d\, E_1(\xi^m)}{d\xi^m}\right|_{\xi=\xi^m} \right) \left(\tfrac{\varepsilon_\xi^c + \alpha_\xi(\xi^m)T_\xi}{c_1(\xi^m)+E_1(\xi^m)^2} \right) \right. \\ & + \left(\left.\tfrac{d}{d\xi}\left(\alpha_\theta(\xi^m)T_\xi\right)\right|_{\xi=\xi^m} + \left.\tfrac{d\varepsilon_\xi^c}{d\xi}\right|_{\xi=\xi^m} + \tfrac{\varepsilon_\theta^c + \alpha_\theta(\xi^m)T - \varepsilon_\xi^c - \alpha_\xi(\xi^m)T_\xi}{\xi^m} \right) \left(\tfrac{c_2(\xi^m)+E_1(\xi^m)E_2(\xi^m)}{c_1(\xi^m)+E_1(\xi^m)^2} \right) \\ & + \left(\left.\tfrac{d}{d\xi}\left(\alpha_\xi(\xi^m)T_\xi\right)\right|_{\xi=\xi^m} + \left.\tfrac{d\varepsilon_\theta^c}{d\xi}\right|_{\xi=\xi^m} + \tfrac{\varepsilon_\xi^c + \alpha_\xi(\xi^m)T_\xi}{\xi^m} \right) \left(\tfrac{c_1(\xi^m)+E_1(\xi^m)^2}{c_1(\xi^m)+E_1(\xi^m)^2} \right) \\ & + \left(\left.\tfrac{d\, c_2(\xi^m)}{d\xi^m}\right|_{\xi=\xi^m} + \left.\tfrac{d}{d\xi^m}\left(E_1(\xi^m)E_2(\xi^m)\right)\right|_{\xi=\xi^m} \right) \left(\tfrac{\varepsilon_\theta^c + \alpha_\theta(\xi^m)T}{c_1(\xi^m)+E_1(\xi^m)^2} \right) - \tfrac{\xi^m \Omega(\xi^m)}{c_1(\xi^m)+E_1(\xi^m)^2} \\ & \left. + \tfrac{1}{\xi^m(c_1(\xi^m)+E_1(\xi^m)^2)} \left(F_1 \left.\tfrac{d\, E_1(\xi^m)}{d\xi^m}\right|_{\xi=\xi^m} - \tfrac{E_2(\xi^m)F_1}{\xi^m} - \left(1 + E_2(\xi^m)^2\right)\left(\varepsilon_\theta^c + \alpha_\theta(\xi^m)T\right) \right) \right). \end{aligned} \tag{18}$$

Hence, the differential equation can now be solved since the terms corresponding to the creep strain functions on the R.H.S have become known. The general solution for Eq. (14) could be written as follows:

$$u_g^m = \underbrace{K_1^m e^{q_1^m \xi}}_{u_{g1}^m} + \underbrace{K_2^m e^{q_2^m \xi}}_{u_{g2}^m}, \tag{19}$$

where

$$q_1^m,\, q_2^m = \frac{-P_2^m \pm \sqrt{(P_2^m)^2 - 4P_3^m P_1^m}}{2P_1^m}. \tag{20}$$

The particular solution of differential Eq. (14) may be obtained according to the Lagrangian method as

$$u_p^m = \xi^{q_1^m} u_1^m + \xi^{q_2^m} u_2^m, \tag{21}$$

where

$$u_1^m = -\int \frac{\xi^{q_2^m}\, R(\xi)|_{\xi=\xi^m}}{W(q_1^m, q_2^m)|_{\xi=\xi^m}}, \qquad u_2^m = \int \frac{\xi^{q_1^m}\, R(\xi)|_{\xi=\xi^m}}{W(q_1^m, q_2^m)|_{\xi=\xi^m}}, \tag{22}$$

in which $R(\xi)$ is the expression on the R.H.S. of Eq. (14) and $W(\xi)$ is defined as

$$W(q_1^m, q_2^m) = \begin{vmatrix} u_{g1}^m & u_{g2}^m \\ (u_{g1}^m)' & (u_{g2}^m)' \end{vmatrix}. \tag{23}$$

The complete solution for u^m in terms of the nondimensional radial coordinate is therefore written as

$$\xi^m - \frac{h^m}{2} \le \xi \le \xi^m + \frac{h^m}{2}, u^m = u_g^m + u_p^m \tag{24}$$

where h^m is the thickness of the mth division. Substituting the displacement from Eq. (24) into Eqs. (10), (11), and (12), the radial and circumferential stresses and electric potential are evaluated.

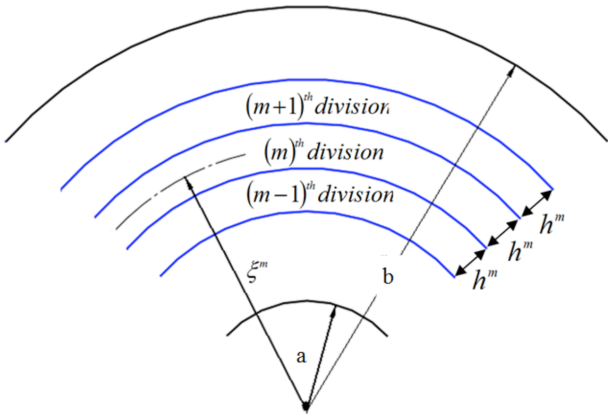

Figure 2. Dividing radial domain into some finite subdomains.

4.1. Heat conduction problem

A distributed temperature field due to steady-state heat conduction without energy generation based on the first law of thermodynamics for the energy equation is given by [6]:

$$\frac{1}{\xi}\left(k(\xi)\,\xi\,T'(\xi)\right)' = 0, \tag{25}$$

where $(')$ denotes differentiation with respect to ξ, and $k = k(\xi)$ is the thermal conductivity. It is assumed that the nonhomogeneous thermal conductivity is also a power-law function of volume fraction, which can be defined in dimensionless form as follows:

$$\overline{k_\xi} = (1-\bar{k})(\frac{\xi-1}{\eta-1})^m + \bar{k}, \quad \bar{k} = \frac{k_a}{k_b}. \tag{26}$$

The nondimensional temperature gradient is defined as

$$\overline{T_\xi} = \frac{T - T_a}{T_b - T_a}, \tag{27}$$

where T_a and T_b are temperatures at the inner and the outer surfaces of the functionally graded cylinder, respectively. Substituting nondimensional variables of Eqs. (26) and (27) into heat conduction Eq. (25) yields

$$\frac{d^2\overline{T_\xi}}{d\xi^2} + (\frac{1}{\xi} + \frac{1}{\overline{K}(\xi)}\frac{d\overline{K}(\xi)}{d\xi})\frac{d\overline{T_\xi}}{d\zeta} = 0. \tag{28}$$

Eq. (28) is a second-order ordinary differential equation (ODE) with variable coefficients. Due to complication of coefficients, a semianalytical method for solution has been used. For this purpose, the solution domain is divided into several divisions (as shown in Figure 2) and the coefficients of Eq. (28) are evaluated at $\xi^{(k)}$, the mean radius of mth division, and the ODE with constant coefficients valid only in mth subdomain turns out to be

$$(\frac{d^2}{d\xi^2} + \overline{c}^{(m)}\frac{d}{d\xi})\overline{T_{\xi^{(m)}}} = 0, \tag{29}$$

where

$$\overline{c}^{(m)} = \frac{1}{\xi^{(m)}} + \frac{1}{\overline{K_{\xi^m}}}\left.\frac{d\overline{K_\xi}}{d\xi}\right|_{\xi=\xi^m}, \quad k = 1, 2, ..., m. \tag{30}$$

Now the second-order ODE with variable coefficients is converted into a second-order ODE with constant coefficients for each division. The exact solution for these types of ODEs can be written as

$$\overline{T_{\xi^{(m)}}} = \overline{X}_1^m + \overline{X}_2^m \exp(-\overline{\xi^m}\overline{c}^{(m)}), \tag{31}$$

where $\overline{X}_1^m$ and $\overline{X}_2^m$ are unknown constants for the mth division. These unknowns are determined by applying the necessary boundary conditions between each two adjacent subdomains.

4.2. Boundary condition

The unknowns $K_1^m, K_2^m, X_1^m, X_2^m, F_1^m$, and F_2^m (the constant of integrating of Eq. (12)) are determined by applying the necessary boundary conditions between two adjacent subdomains. For this purpose, the continuity of radial displacement, radial stress, temperature, and electric potential are imposed at the interfaces of the adjacent subdomains. These continuity conditions at the interfaces are

$$\begin{aligned}
&u^m\big|_{\xi=\xi^m+\frac{h^m}{2}} = u^{m+1}\big|_{\xi=\xi^{m+1}-\frac{h^{m+1}}{2}},\\
&\left.\frac{du^m}{d\xi}\right|_{\xi=\xi^m+\frac{h^m}{2}} = \left.\frac{du^{m+1}}{d\xi}\right|_{\xi=\xi^{m+1}-\frac{h^{m+1}}{2}},\\
&\sigma_r^m\big|_{\xi=\xi^m+\frac{h^m}{2}} = \sigma_r^{m+1}\big|_{\xi=\xi^{m+1}-\frac{h^{m+1}}{2}},\\
&\Phi^m\big|_{\xi=\xi^m+\frac{h^m}{2}} = \Phi^{m+1}\big|_{\xi=\xi^{m+1}-\frac{h^{m+1}}{2}},\\
&\left.T_\xi^m\right|_{\xi=\xi^m+\frac{h^m}{2}} = \left.T_\xi^m\right|_{\xi=\xi^{m+1}+\frac{h^{m+1}}{2}},\\
&\left.\frac{\partial T_\xi^m}{\partial\xi}\right|_{\xi=\xi^m+\frac{h^m}{2}} = \left.\frac{\partial T_\xi^m}{\partial\xi}\right|_{\xi=\xi^{m+1}+\frac{h^{m+1}}{2}},
\end{aligned} \tag{32}$$

and global boundary conditions are written in dimensionless form as

$$\sigma_\xi(\eta) = 0\sigma_\xi(1) = -1, \quad \Phi(1) = 1, \quad \Phi(\eta) = 0, \quad T_\xi(1) = 1, \quad T_\xi(\eta) = 0. \tag{33}$$

The continuity conditions of Eq. (32) together with the global boundary conditions of Eq. (33) yield a set of linear algebraic equations in terms of $K_1^m, K_2^m, X_1^m, X_2^m, B_1^m$, and B_2^m. By solving the resultant linear algebraic

equations, the unknown coefficients can be calculated. Then the displacement component, the stresses, and the electric potential are determined in each radial subdomain. Increasing the number of divisions improves the accuracy of the results.

5. Time-dependent thermoelectroelastic creep behavior of the cylinder

To obtain time-dependent stresses and electric potential, the creep strains in Eqs. (10), (11), and (12) must be considered. Creep strain rates are related to the material creep constitutive model and the current stress tensor by the well-known Prandtl–Reuss relation. In this case, the Prandtl–Reuss relation is written as [23]:

$$\dot{\varepsilon}_r = \frac{\dot{\varepsilon}_e}{\sigma_e}\left[\sigma_r - 0.5\left(\sigma_\theta + \sigma_z\right)\right], \tag{34}$$

$$\dot{\varepsilon}_\theta = \frac{\dot{\varepsilon}_e}{\sigma_e}\left[\sigma_\theta - 0.5\left(\sigma_r + \sigma_z\right)\right], \tag{35}$$

$$\dot{\varepsilon}_z = \frac{\dot{\varepsilon}_e}{\sigma_e}\left[\sigma_z - 0.5\left(\sigma_\theta + \sigma_r\right)\right]. \tag{36}$$

For plane strain condition the axial strain rate disappears, i.e. $\dot{\varepsilon}_z = 0$.

$$\sigma_z = 0.5\left(\sigma_\theta + \sigma_r\right). \tag{37}$$

Substituting Eq. (37) into the first two of Eqs. (34) and (35), the radial and circumferential strain rates are found to be

$$\dot{\varepsilon}_r = \frac{3\dot{\varepsilon}_e}{4\sigma_e}\left(\sigma_r - \sigma_\theta\right), \tag{38}$$

$$\dot{\varepsilon}_\theta = \frac{3\dot{\varepsilon}_e}{4\sigma_e}\left(\sigma_\theta - \sigma_r\right). \tag{39}$$

The Bailey–Norton creep constitutive model for FGPM is considered to be [24]

$$\dot{\varepsilon}_e = Bt^n\sigma_e^{n(r)}, \tag{40}$$

where B and m are the Norton coefficient and n is the Bailey coefficient, for which $\frac{1}{2} < n < \frac{1}{3}$.

In this case, the Von Mises equivalent stress is reduced to

$$\sigma_e = \frac{1}{\sqrt{2}}\sqrt{\left(\sigma_\theta - \sigma_r\right)^2 + \left(\sigma_\theta - \sigma_z\right)^2 + \left(\sigma_z - \sigma_r\right)^2} = \frac{\sqrt{3}}{2}\left(\sigma_\theta - \sigma_r\right). \tag{41}$$

To obtain a history of stresses, deformation, and electric potential, a numerical procedure based on the method of successive approximation has been tailored.

6. Successive approximation method

As can be seen from the above, to obtain the history of stresses, strains, deformation, and electric potential, a numerical procedure based on the method of successive approximation has been adopted, for which a procedure based on Mendelson's method is described below.

1. An appropriate time increment step of say $\Delta t = 6$ months is selected. The total time is therefore the sum of time increments throughout the progress of the creep process. For the ith timing step, the total time is
$$t_i = \sum_{k=1}^{i-1} \Delta t_k + \Delta t_i.$$

2. Thickness of the cylinder is divided into N equal divisions. Initial estimates are $\Delta\varepsilon^c_{r,ij} = -0.00001$ and $\Delta\varepsilon^c_{\theta,ij} = 0.00001$ for radial and circumferential creep strain increments to be considered for all division points throughout the thickness. Creep strain at any point throughout the thickness of the cylinder is the cumulative sum of all previous creep strains. Hence,
$$\varepsilon^c_{r,ij} = \sum_{k=1}^{i-1} \Delta\varepsilon^c_{r,kj} + \Delta\varepsilon^c_{r,ij}, \varepsilon^c_{\theta,ij} = \sum_{k=1}^{i-1} \Delta\varepsilon^c_{\theta,kj} + \Delta\varepsilon^c_{\theta,ij},$$
where the subscripts i and j indicate the timing step and division point, respectively.

3. First- and second-order derivatives of radial and circumferential creep strains are calculated using finite difference approximation as follows:
$$\frac{\partial\varepsilon^c_{r,im}}{\partial\xi_m} = \frac{\varepsilon^c_{r,im+1} - \varepsilon^c_{r,im-1}}{2\ h^m},$$
$$\frac{\partial\varepsilon^c_{\theta,im}}{\partial\xi_m} = \frac{\varepsilon^c_{\theta,im+1} - \varepsilon^c_{\theta,im-1}}{2\ h^m},$$
$$\frac{\partial^2\varepsilon^c_{r,im}}{(\partial\xi^2_m)} = \frac{\varepsilon^c_{r,im+1} - 2\varepsilon^c_{r,im} + \varepsilon^c_{r,im-1}}{(h^m)^2},$$
$$\frac{\partial^2\varepsilon^c_{\theta,im}}{\partial\xi^2_m} = \frac{\varepsilon^c_{\theta,im+1} - 2\varepsilon^c_{\theta,im} + \varepsilon^c_{\theta,im-1}}{(h^m)^2}.$$

4. The cumulative creep strains and its first-order derivatives are substituted in Eq. (14). This differential equation can be solved for the displacement at the mth layer. Then using second-order derivatives stresses and electric potential are calculated at the same layer. Using local and global boundary conditions, the displacements, stresses, and electric potentials at time t_i are determined.

5. Effective stresses are calculated for all division points using $\sigma_{e,ij} = \frac{\sqrt{3}}{2}\left|\sigma_{\theta,ij} - \sigma_{r,ij}\right|$.

6. Effective creep strain rates are then calculated at all division points (j) for the ith timing step using the Bailey–Norton creep constitutive model using $\dot{\varepsilon}_{e,ij} = B\, t_i^n \sigma_{e,ij}^m$.

7. From the Prandtl–Reuss relation, radial and circumferential creep strain rates are obtained:
$$\dot{\varepsilon}_{r,ij} = \frac{3\dot{\varepsilon}_{e,ij}}{4\sigma_{e,ij}}\left(\sigma_{r,ij} - \sigma_{\theta,ij}\right),$$
$$\dot{\varepsilon}_{\theta,ij} = \frac{3\dot{\varepsilon}_{e,ij}}{4\sigma_{e,ij}}\left(\sigma_{\theta,ij} - \sigma_{r,ij}\right).$$

8. New values for radial and circumferential creep strain increments at all division points are recalculated using the above creep strain rates (stage 6) and the time increment

$$\Delta\varepsilon_{r,ij}^{c,new} = \dot{\varepsilon}_{r,ij}^{c} \times \Delta t_i,$$

$$\Delta\varepsilon_{\theta,ij}^{c,new} = \dot{\varepsilon}_{\theta,ij}^{c} \times \Delta t_i.$$

9. These new obtained values for creep strain increments are compared with the first estimate and if needed replace it, and the procedure is repeated until the required convergence is achieved. When considering the next time step, the first estimate of creep strain should be the converged value obtained from the previous step time, and again the procedure is repeated from stage 2 above.

7. Numerical results and discussion

The numerical results presented here are based on the material properties defined in Table 1 for PZT_4 as the inner surface and PZT_5 as the outer surface [25]. The temperature at the inner and outer surfaces of the FGPM cylinder are considered to be $T_a = 50\ ^\circ\mathrm{C}$ and $T_b = 25\ ^\circ\mathrm{C}$, respectively, and the aspect ratio is $\eta = 1.3$. The final converged solutions using the numerical procedure outlined in Section 6 above are illustrated as histories of stresses, displacement, and electric potential in Figures 3–10.

Table 1. Mechanical, electrical, and thermal properties for PZT_5 and PZT_4.

Property	PZT_5		PZT_4	
c_{11}	131	Gpa	115	Gpa
c_{12}	81.3	Gpa	74.3	Gpa
c_{22}	148	Gpa	139	Gpa
e_{11}	9.50	C/m^2	77.8	Gpa
e_{12}	–2.10	C/m^2	15.1	C/m^2
e_{11}	9.4×10^{-9}	C^2/Nm^2	-5.2	C/m^2
	1×10^{-6}	$1/k$	3.87×10^{-9}	F/m
α_{r0}	2×10^{-6}	$1/k$	2×10^{-5}	$1/K$
ρ	7600	kg/m^3	2×10^{-6}	$1/K$

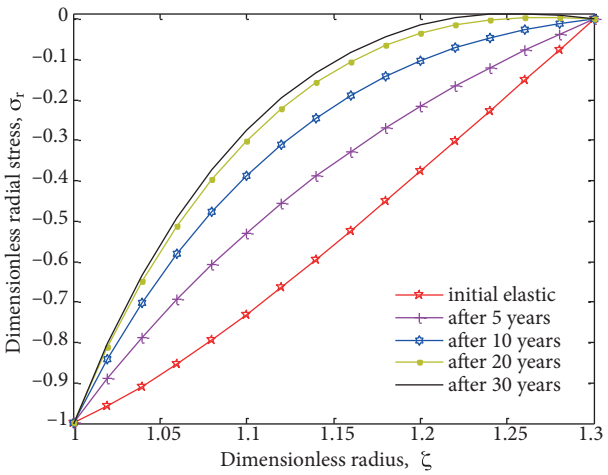

Figure 3. History of radial stress for the FGPM cylinder from initial elastic up to 30 years for the case $n = 2$.

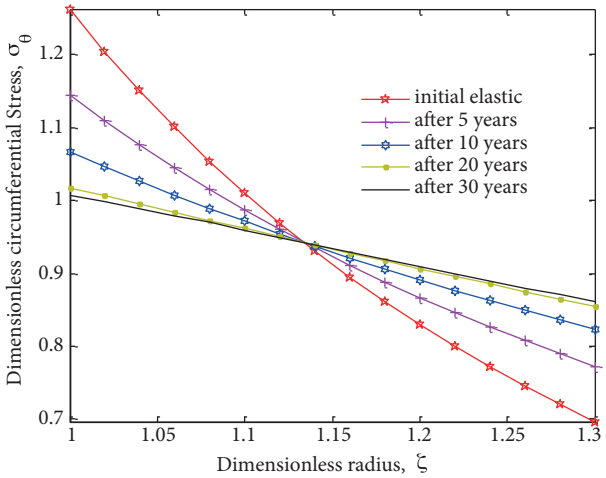

Figure 4. History of circumferential stress for the FGPM cylinder from initial elastic up to 30 years for the case $n = 2$.

Table 2 illustrates the effects of grading index and time-dependent creep on dimensionless effective stress versus dimensionless radius. As can be seen, the maximum effective stress belongs to $n = 0$ (PZT_5) and the minimum values belong to $n = Infinity$ (PZT_4), and for the FGPM cylinder these values are located between these two extremes. Furthermore, the change in the rate of effective stress become less significant after 10, begins to converge after 20, and reaches the steady state after 30 years. The results of this paper for a homogeneous piezoelectric cylinder ($n = 0$) are the same as those reported by Ghorbanpour et al. [6], indicating the validation of present work.

Table 2. Effects of grading index and time-dependent creep on dimensionless effective stress versus dimensionless radius.

Dimensionless radius (ξ)	Grading index ($\boldsymbol{n}$)	Time				
		Initial elastic	After 5 years	After 10 years	After 20 years	After 30 years (steady state)
1.06	0[1]	2.4384	2.4302	2.4246	2.4217	2.4204
	0.5	1.9698	1.9622	1.9572	1.9541	1.9534
	2	1.5624	1.5563	1.5528	1.5487	2.5477
	5	1.5561	1.5488	1.5419	1.5389	1.5381
	Infinity	1.5452	1.5377	1.5309	1.5284	1.5278
1.12	0[1]	2.1357	2.1807	2.2107	2.2257	2.2316
	0.5	1.6529	1.6991	1.7109	1.7257	1.7219
	2	1.2462	1.2808	1.3115	1.3248	1.3241
	5	1.2398	1.2712	1.2986	1.3070	1.3037
	Infinity	1.2287	1.2734	1.2854	1.2949	1.2906
1.24	0[1]	1.6534	1.7308	1.7824	1.8082	1.8185
	0.5	1.1187	1.1889	1.2348	1.2601	1.2711
	2	0.7782	0.8481	0.8990	0.9128	0.9212
	5	0.6298	1.7422	1.7920	1.8122	1.8021
	Infinity	0.6221	1.7392	1.7827	1.8078	1.7952

Figure 3 demonstrates histories of dimensionless radial stress (σ_r) against a dimensionless radius (ξ) for the case $n = 2$. This figure shows that throughout the cylinder thickness, the absolute value of radial stress decreases with time. Maximum change in σ_r occurs in the midrange of ξ. The change in the rate of radial stress becomes less significant after 10, begins to converge after 20, and reaches steady state after 30 years. Furthermore, radial stresses are constant with respect to time at the interior and exterior surfaces of the cylinder, satisfying the constant mechanical boundary conditions set out originally in Eq. (33).

Figures 4–6 illustrate the plots of circumferential, longitudinal, and effective stresses across the cylinder thickness for the case $n = 2$. As can be seen, all these stresses are positive, i.e. they remain tensile throughout the thickness. As far as the effect of time on these stresses is concerned, they are decreasing at the inner surface of the FGPM cylinder and increasing at the outer surface with decreasing rates so that they also approach steady-state condition after 30 years. Reference stresses are also identified for these stresses, which are independent of time. The maximum longitudinal stress occurs at the outer surface, while the maximum circumferential and effective stresses occur at the inner surface of the cylinder.

Despite different (but satisfied) boundary conditions at the inner and outer surfaces (see Eq. (33)), the histories of the imposed electric potential through-thickness, as shown in Figure 7 for the case $n = 2$, are fairly similar to that of the compressive radial stress as far as the rate change is concerned. That is perhaps because

the electric potential histories are induced by the compressive radial stress histories during creep deformation of the cylinder. This is expected from the piezoelectric characteristic point of view.

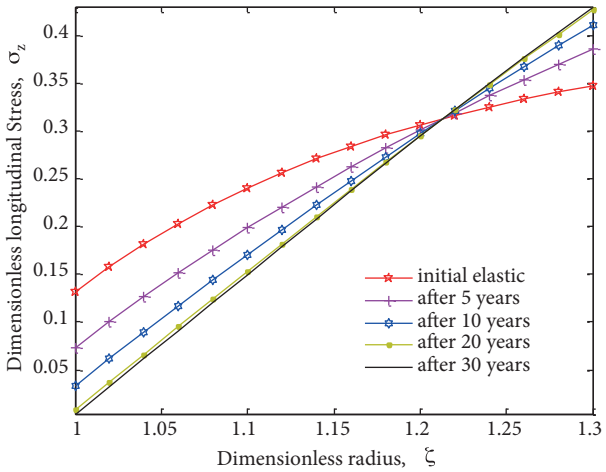

Figure 5. History of longitudinal stress for the FGPM cylinder from initial elastic up to 30 years for the case $n = 2$.

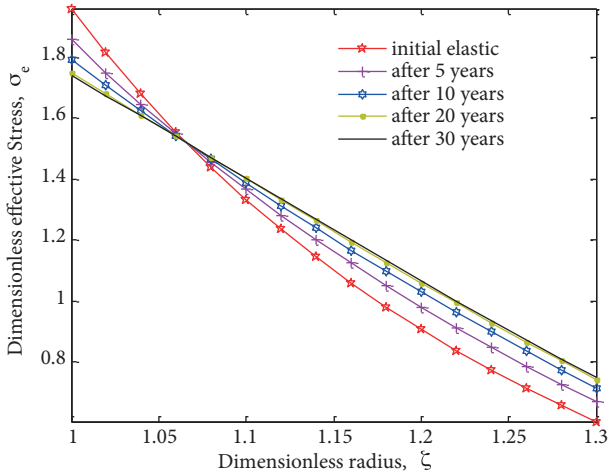

Figure 6. History of effective stress for the FGPM cylinder from initial elastic up to 30 years for the case $n = 2$.

History of radial displacements, u, is shown in Figure 8 for the case $n = 2$. It is clear that u increases with time at a decreasing rate during the creep process of the cylinder and finally reaches a steady state at 30 years, the same as σ_i $(i = r, \theta, z)$, Φ. Minimum u occurs at the interior surface and it increases smoothly towards the exterior.

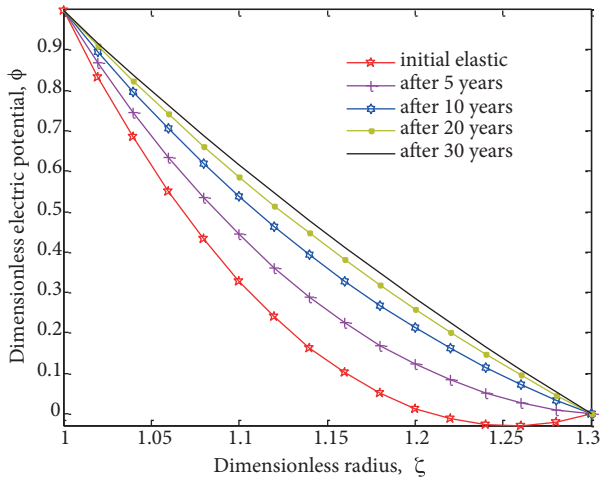

Figure 7. History of electric displacement for the FGPM cylinder from initial elastic up to 30 years for the case $n = 2$.

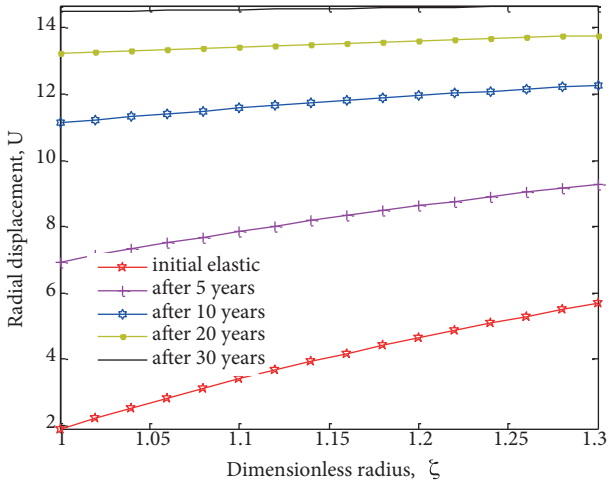

Figure 8. History of radial displacement for the FGPM cylinder from initial elastic up to 30 years for the case $n = 2$.

As for the histories of radial and circumferential creep strains, these are presented in Figures 9 and 10 for the case $n = 2$. The radial and tangential strains are equal in magnitude but opposite in nature (sign) due to the incompressibility condition $(\dot{\varepsilon}_r + \dot{\varepsilon}_\theta + \dot{\varepsilon}_z = 0)$ and the assumption of plain strain condition $(\dot{\varepsilon}_z = 0)$.

The absolute value of both creep strains with time is much higher at the interior surface as compared with the exterior. As far as the rate of change is concerned, this seems to increase to a maximum between 5 and 10 years, and then decreases until it reaches steady state around 30 years of operation.

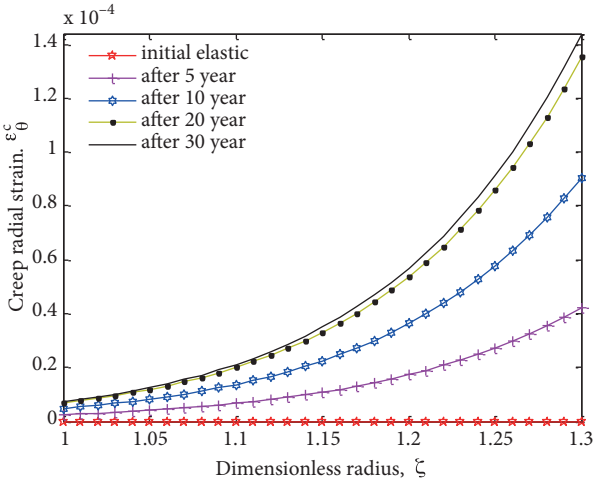

Figure 9. History of radial creep strain stress for the FGPM cylinder from initial elastic up to 30 years for the case $n = 2$.

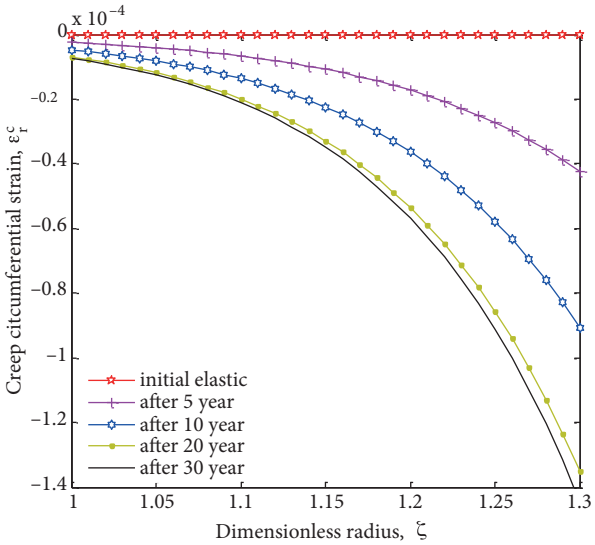

Figure 10. History of circumferential creep strain stress for the FGPM cylinder from initial elastic up to 30 years for the case $n = 2$.

8. Conclusions

Time-dependent creep analysis has been carried out to improve the performance and reliability of piezoactuators used for high-precision applications, when these devices are used even at room temperatures. Time-dependent thermoelectromechanical creep behavior of radially polarized FGPM hollow rotating cylinder was investigated using a successive approximation method based on the Bailey–Norton law. History of stresses, strains, electric potentials, and displacements were studied and presented graphically. Creep behavior of these is fairly similar as changes in the rates for these become less significant after 10, begin to converge after 20, and reach steady state after 30 years of operation. The results show that the grading index has a significant effect on the thermoelectromechanical creep stresses, electric potential, and radial displacement. In general, a major redistribution for electric potential takes place throughout the thickness. Electric potentials are increasing with time in the same direction as the compressive radial stress histories. The histories of the imposed electric potential through-thickness are fairly similar to that of the compressive radial stress as far as the rate change is concerned, which is expected, as the electric potential histories of piezoelectric material are induced by the compressive radial stress histories during creep deformation of the cylinder, justifying its industrial application for efficient actuators and sensors.

Acknowledgments

The author would like to thank the reviewers for their comments and suggestions to improve the clarity of this article. The authors are grateful to the University of Kashan for supporting this work by Grant No. 363443/14.

References

[1] Jabbari M, Sohrabpour S, Eslamic MR. Mechanical and thermal stresses in a functionally graded hollow cylinder due to radially symmetric loads. Int J Press Ves Pip 2002: 79; 493–497.

[2] Liew KM, Kitipornchai S, Zhang XZ, Lim CW. Analysis of the thermal stress behaviour of functionally graded hollow circular cylinders. Int J Solids Struct 2003; 40: 2355–2380.

[3] You LH, Zhang JJ, You XY. Elastic analysis of internally pressurized thick-walled spherical pressure vessels of functionally graded materials. Int J Press Ves Pip 2005; 82: 347–354.

[4] Dai HL, Fu YM, Dong ZM. Exact solutions for functionally graded pressure vessels in a uniform magnetic field. Int J Solids Struct 2006; 43: 5570–5580.

[5] Bahtui A, Eslami MR. Coupled thermoelasticity of functionally graded cylindrical shells. Mech Res Commun 2007; 34: 1–18.

[6] Ghorbanpour Arani A, Kolahchi R, Mosallaei Barzoki AA. Effect of material in-homogeneity on electro-thermo-mechanical behaviors of functionally graded piezoelectric rotating shaft. Appl Math Model 2011; 35: 2771–2789.

[7] Ghorbanpour Arani A, Kolahchi R, Mosallaie Barzoki AA, Loghman A. Electro-thermo-mechanical behaviors of FGPM spheres using analytical method and ANSYS software. Appl Math Model 2011; 36: 139–157.

[8] Pai DH. Steady-state creep analysis of thick-walled orthotropic cylinders. Int J Mech Sci 1967; 9: 335–482.

[9] Sim RG, Penny RK. Plane strain creep behaviour of thick-walled cylinders. Int J Mech Sci 1971; 13: 987–1009.

[10] Bhatnagar NS, Arya VK. Large strain creep analysis of thick-walled cylinders. Int J Non-Linear Mech 1974; 9: 127–40.

[11] Simonian AM. Calculation of thermal stresses in thick-walled cylinders taking account of non-linear creep. Int J Eng Sci 1979; 17: 513–522.

[12] Yang YY. Time-dependent stress analysis in functionally graded materials. Int J Solids Struct 2000; 37: 7593–7608.

[13] Altenbach H, Gorash Y, Naumenko K. Steady-state creep of a pressurized thick cylinder in both the linear and the power law ranges. Acta Mech 2008; 195: 263–274.

[14] Loghman A, Ghorbanpour Arani A, Amir S, Vajedi A. Magnetothermoelastic creep analysis of functionally graded cylinders. Int J Press Ves Pip 2010; 87: 389–395.

[15] Loghman A, Aleayoub SMA, Hasani Sadi M. Time-dependent magnetothermoelastic creep modeling of FGM spheres using method of successive elastic solution. Appl Math Model 2012; 36: 836–845.

[16] Ghorbanpour Arani A, Mosallaie Barzoki AA, Kolahchi R, Mozdianfard MR, Loghman A. Semi-analytical solution of time-dependent electro-thermo-mechanical creep for radially polarized piezoelectric cylinder. Comput Struct 2011; 89: 1494–1502.

[17] Dai HL, Jiang HJ, Yang L. Time-dependent behaviors of a FGPM hollow sphere under the coupling of multi-fields. Solid State Sci 2012; 14: 587–597.

[18] Ghorbanpour Arani A, Kolahchi R, Mosallaie Barzoki AA, Loghman A. Electro-thermo-mechanical creep and time-dependent behavior of FGPM spheres. Turkish J Eng Env Sci 2012; 38: 208-218.

[19] Zhou D, Kamlah M. Room-temperature creep of soft PZT under static electrical and compressive stress loading. Acta Mat 2006; 54: 1389–1396.

[20] Tiersten HF. Linear Piezoelectric Plate Vibrations. New York, NY, USA: Plenum Press, 1976.

[21] Kordkheili SAH, Naghdabadi R. Thermoelastic analysis of a functionally graded rotating disk. Comput Struct 2007; 79: 508–516.

[22] Bayat M, Saleem M, Sahari BB, Hamouda AMS, Mahdi E. Mechanical and thermal stresses in a functionally graded rotating disk with variable thickness due to radially symmetry loads. Int J Press Ves Pip 2009; 86: 357–372.

[23] Penny RK, Marriott DL. Design for Creep. London, UK: Chapman & Hall, 1995.

[24] Norton FH. The Creep of Steel at High Temperatures. London, UK: McGraw-Hill; 1929.

[25] Jaffe H, Berlincourt DA. Piezoelectric transducer materials. P IEEE 1965; 53: 1372–1386.